JOURNAL OF MATERIALS SCIENCE 15 (1980) 415–425

X-ray line broadening study of splat-quenched Ag-Sn alloys

A. M. TONEJC, A. BONEFAČIĆ
Institute of Physics of the University, Zagreb, Yugoslavia

Microstrains, effective particle sizes, and stacking fault probabilities were determined by analysis of X-ray powder pattern peaks of splat-quenched Ag–6 at % Sn, Ag–8.2 at % Sn and Ag–11 at % Sn alloys.

The shapes and positions of all available (*h k l*) reflections for Cu$K\alpha$ radiation were recorded, using focusing Bragg–Brentano X-ray geometry. To measure peak positions, Co$K\alpha$ radiation and a Seeman–Bohlin camera were used with an internal standard.

Fourier analysis and Stokes correction were used. The separation of particle sizes and microstrain components was performed using the Warren–Averbach and the single-profile methods. Errors arising during the separation of particle sizes and microstrains from an inaccurate estimation of background intensity, and the influence of standards with different annealing treatments, were considered.

The particle sizes and microstrains were found to be anisotropic. This anisotropy was due to the presence of stacking faults and an irregular distribution of dislocations in as-quenched samples. Peak shift analysis showed that some macrostresses remained after plastic deformation caused by quenching. It appears that better quenching produces thinner samples and higher macrostresses. The particle sizes, microstrains and compound stacking fault probabilities were compared with corresponding values for cold-worked filings and bulk compressed alloys.

1. Introduction

By rapid quenching from the melt a high concentration of defects may be quenched in [1, 2], and if the two-piston quenching technique is used [3], quenched samples may become plastically deformed to an unknown degree during quenching [4]. The droplets of liquid alloy, injected between two rapidly moving pistons, are not only squeezed between them, but, after complete solidification, solid samples may undergo a certain plastic deformation caused by the shock of the pistons in collision.

The purpose of the present investigation was to make a detailed X-ray analysis of an alloy, quenched by the two-piston method, as regards crystallite size, lattice strains, and lattice stacking faults, and compare it both with the results obtained from analysing bulk Ag–Sn specimens deformed in compression [5], and with cold-worked Ag–Sn filings [6, 7]. A detailed analysis of the shifts in the position of diffraction peaks was made in order to prove the presence of residual stresses remaining after plastic deformation during rapid quenching.

For the separation of particle sizes and microstrains two independent methods were used: the Warren–Averbach and the single-profile methods. Errors arising from an inaccurate estimation of the background intensity and from the use of standards with different annealing treatments were examined.

2. Experimental procedure

Three silver–tin alloys, Ag–6 at % Sn, Ag–8.2 at % Sn and Ag–11 at % Sn (Ag 6 Sn, Ag 8.2 Sn, Ag 11 Sn), were prepared from spectrographically standardized silver and tin. The details of the experimental arrangements have been described previously [4]. The ingots were rapidly quenched from the melt by the two-piston method and by the piston and anvil technique [3]. Powder-pattern

0022–2461/80/020415–11$03.10/0

peaks were measured with a diffractometer using Cu$K\alpha$ radiation, and a Seeman–Bohlin camera using Co$K\alpha$ radiation. Cu$K\alpha$ radiation was monochromated using a bent quartz crystal, which focused it on the entrance slit of the scintillation counter, and it was registered using a Siemens diffractometer, a scintillation detector and an oscillating attachment. The experimental conditions included the use of an 0.7° divergence slit and an 0.1 mm receiving slit. All peaks were step-scanned with a speed of 0.02° min^{-1}, while the chart speed was 0.005° mm^{-1}.

All the identifiable peaks were analysed. For profiles (1 1 1), (2 0 0) and (2 2 2) the data were read from the chart at intervals of 0.005° in 2θ, and for profile (4 0 0) at intervals of 0.010° in 2θ. Fourier analysis of the line broadening was preferred to integral breadth, since the former yields more details about microstrain distribution, and no assumption is required regarding the shapes of peaks. The Fourier coefficients of the line profiles of the quenched samples were corrected for instrumental broadening by the Stokes method [8], using the same but well annealed sample as a standard. The isochronal annealing procedure was used. The specimens of each of the three alloys were annealed in vacuum for 15 min at different temperatures (from 25° C to 500° C).

In order to evaluate the errors arising from the separation of particle sizes and microstrains two different standards were used (for Ag 8.2 at % Sn). The first (1S) was a specimen of the same concentration as the as-quenched sample annealed isochronally at intervals of 50° C in vacuum for 15 min at different temperatures from (25° C to 500° C). The second standard (2S) was of the same concentration as the as-quenched sample, but annealed longer than the first standard (2 h at 500° C).

3. Analysis of diffraction data

3.1. Line broadening

Fourier analysis of the broadened peaks, and the Stokes correction for instrumental broadening, were made using a computer program written in Fortran.

The method of Warren and Averbach [9] and the single profile method [10] were used to separate the strain term and the particle size term [11, 12, 13]. The Fourier coefficients $A(L)$ can be written in the form

$$A(L) = A^{p}(L)A^{\epsilon}(L), \qquad (1)$$

where the peak maximum is used as the origin of the Fourier integral, and the superscripts p and ϵ represent the particle size and strain components of each coefficient. $A^{p}(L)$ and $A^{\epsilon}(L)$ can be approximated for small values of L to

$$A^{p}(L) = 1 - \frac{L}{D_{ehkl}} = 1 - L\left(\frac{1}{D} + \frac{1.5\alpha + \beta}{a} V_{hkl}\right) \qquad (2)$$

$$A^{\epsilon}(L) = 1 - 2\pi^2 L^2 \langle \epsilon_L^2 \rangle_{hkl} \times \frac{h_0}{a^2},$$

where L is the distance normal to the reflecting planes $(h\,k\,l)$ of the interplanar spacing $(h\,k\,l)$, D_{ehkl} is the effective particle size, D is the true particle size and α is the deformation stacking fault probability, defined by $\alpha = \alpha' + \alpha''$, α' is the intrinsic stacking fault probability, α'' is the extrinsic stacking fault probability, β is the twin stacking fault probability, $\langle \epsilon_L^2 \rangle$ is the mean square strain (MSS) component normal to the reflecting planes $(h\,k\,l)$, V_{hkl} is the constant for a given direction [13], a is the lattice parameter, and $h_0 = h^2 + k^2 + l^2$.

Applying the single-profile method in the manner of Mignot and Rondot [14] it has been assumed that $\epsilon_n^2 = C/n$, and that the nth Fourier coefficients $A(n)$ can be written as follows:

$$A(n) = (1 - nx) \times (1 - n^2 y_n)$$

$$= 1 - n(x + KC) + n^2 xKC,$$

where

$$x = \tfrac{1}{2}[-a_1 \pm (a_1^2 - 4a_2)^{1/2}],$$

$$C = \frac{a_2}{xK}.$$

$A(n)$ may be approximated by the polynomial $P(n) = a_0 + a_1 n + a_2(n^2)$, where a_0, a_1 and a_2 are the coefficients of the polynomial $P(n)$.

The effective particle size is $D_e = \delta/x$, where δ is a distance whose magnitude is inversely proportional to the Fourier period, and $K = 2\pi^2\delta^2/d^2$, where d is the distance between the $(h\,k\,l)$ planes. The approximation of $A(n)$ by the polynomial was performed so that the least square fit of

$$\sum_{n_0}^{N} [A(n) - P(n)]^2$$

was a minimum. N is the total number of the Fourier coefficients used in the calculation, and n_0 is the smallest utilized value of Fourier's harmonic. The results were selected whilst apply-

TABLE I Measured particle sizes D_{ehkl}, D, r.m.s. strains $\langle\epsilon_L^2\rangle_{hkl}^{1/2}(L = 50\,\text{Å})$ and compound stacking fault probabilities $(1.5\alpha + \beta)$ and $(\beta + 4.5\alpha'')$ in splat-quenched Ag–Sn alloys.

	$\langle\epsilon_L^2\rangle_{111}^{1/2} \times 10^3$	$\langle\epsilon_L^2\rangle_{100}^{1/2} \times 10^3$	D_{e111}(Å)	D_{e100}(Å)	D(Å)	$(1.5\alpha + \beta)$	$(\beta + 4.5\alpha'')$
Ag 6 Sn	0.85	1.06	1200	900	1650	0.002	0.0038
Ag 8.2 Sn	1.70	2.20	520	380	1330	0.007	0.0055
Ag 11 Sn	1.44	2.34	770	510	1450	0.005	0.0113

ing the following conditions:

$$a_0 \approx 1, \quad a_2 > 0$$

and

$$\frac{1}{N}\sum_{n_0}^{N}[A(n) - P(n)]^2 = \text{minimum}.$$

The experimental results obtained from line profile analysis on splat-quenched samples of three Ag–Sn alloys are presented in Table I and Figs. 1a and b, 2a and b.

3.1.1. Errors arising in separation of particle sizes and microstrains

The choice of background was a problem for line (4 0 0) since it was very broad and of low intensity. In order to evaluate the truncation error calculations were made using two different background levels. The second level was obtained by lowering the first by about 10 per cent of the (4 0 0) peak maximum value. No variation of the background levels of lines (2 0 0), (1 1 1) and (2 2 2) was

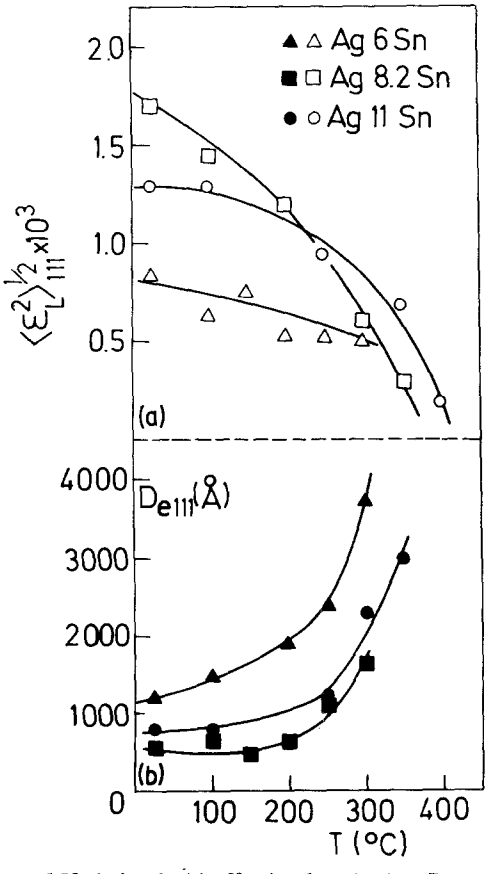

Figure 1 Variation in (a) effective domain sizes D_{e111} and (b) r.m.s. strains $\langle\epsilon_L^2\rangle^{1/2}(L = 50\,\text{Å})$, in direction [1 1 1], after 15 min isochronal annealing in Ag–Sn splat-quenched alloys: (a) ▲ Ag 6 Sn, ■ Ag 8.2 Sn, ● Ag 11 Sn; (b) △ Ag 6 Sn, □ Ag 8.2 Sn, ○ Ag 11 Sn.

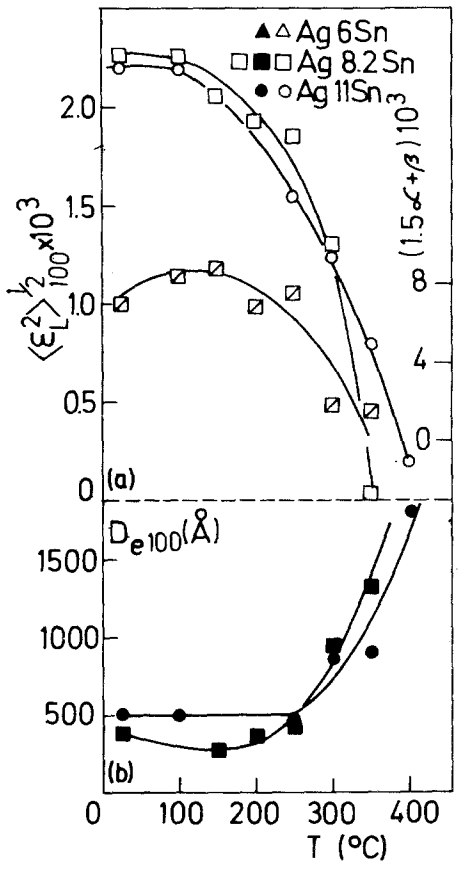

Figure 2 Variation in (a) effective domain sizes D_{e100} and (b) r.m.s. strains $\langle\epsilon_L^2\rangle^{1/2}$ (at $L = 50$ Å), in direction [1 0 0] and compound stacking fault probability $(1.5\alpha + \beta)$ after 15 min isochronal annealing in Ag–Sn splat-quenched alloys: (a) ■ Ag 8.2 Sn, ● Ag 11 Sn, (b) □ Ag 8.2 Sn, ○ Ag 11 Sn, ▨ Ag 8.2 Sn $(1.5\alpha + \beta)$.

TABLE II Measured values of D_{e100} and $\langle\epsilon_L^2\rangle_{100}^{1/2}$ (L = 50 Å) separated according to the Warren–Averbach method by means of two different standards and two background levels of line (4 0 0), for different annealing temperatures.

		Temperature (° C)					
		23	150	200	250	300	350
First standard	$D_{e100}(1)$ (Å)	350	250	300	420	–	–
(1S)	$D_{e100}(2)$ (Å)	420	265	420	485	1010	–
	$\langle\epsilon_{50}^2\rangle_{100}^{1/2}(1) \times 10^3$	1.30	0	0.80	0.82	0	–
	$\langle\epsilon_{50}^2\rangle_{100}^{1/2}(2) \times 10^3$	2.20	2.0	1.95	1.85	1.18	–
Second standard	$D_{e100}(1)$ (Å)	320	240	310	360	900	–
(2S)	$D_{e100}(2)$ (Å)	380	260	380	450	950	1320
	$\langle\epsilon_{50}^2\rangle_{100}^{1/2}(1) \times 10^3$	1.20	0	0.90	0.83	0	–
	$\langle\epsilon_{50}^2\rangle_{100}^{1/2}(2) \times 10^3$	2.25	2.10	1.90	1.85	1.20	–

undertaken. After the Warren–Averbach analysis the Stokes-corrected Fourier coefficients obtained, with two different standards, gave effective domain sizes, $D_{e100}(1)$ and root mean square (r.m.s.) strains $\langle\epsilon_L^2\rangle_{100}^{1/2}(1)$ (for the higher intensity level, i.e. corrected background level) and $D_{e100}(2)$ and $\langle\epsilon_L^2\rangle_{100}^{1/2}(2)$ (for the lower intensity level). The results are shown in Figs. 3, 4, 5 and 6 and Table II. Figs. 3 and 4 show the effective domain sizes D_{e100} and D_{e111} against annealing temperature, obtained from the slopes of the curves of the particle size coefficients A_L^S against L, for values of L between 25 Å and 200 Å (for all the lines).

Fig. 4 shows the effective domain sizes in the [1 1 1] direction against the temperature of annealing obtained by using two different standards, (1S) and (2S).

As can be seen from Fig. 3 and Table II in the [1 0 0] direction, for both standards and for all annealing temperatures, the values of effective domain sizes obtained with a higher background intensity level were smaller by between 10 and 20 per cent. This result is in agreement with the findings of Gili and Borea [15], who examined the truncation errors of simulated profiles with a supposed degree of deformation. They found that even a truncation error of the second-order reflex gives domain sizes smaller than the true ones, while the truncation of the first-order reflex

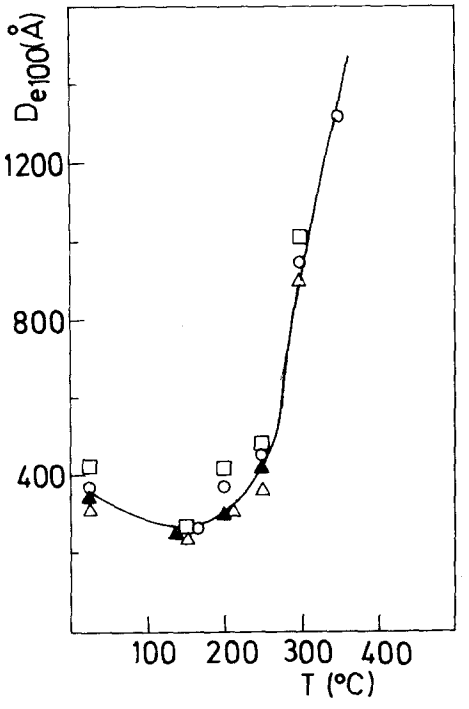

Figure 3 The effective domain sizes D_{e100} in direction [1 0 0] (marked (1) for higher intensity level, and (2) for lower intensity level) obtained from two background levels of line (4 0 0) by means of two different standards (1S and 2S) versus annealing temperature T(° C): ▲ D_{e100} (1) 1S, △ D_{e100}(1) 2S, □ D_{e100}(2) 1S, ○ D_{e100}(2) 2S.

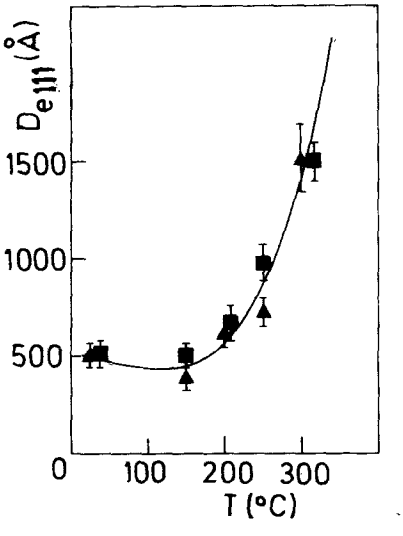

Figure 4 The effective domain sizes D_{e111} in direction [1 1 1] obtained with two different standards (1S and 2S): ■ D_{e111} 1S, ▲ D_{e111} 2S.

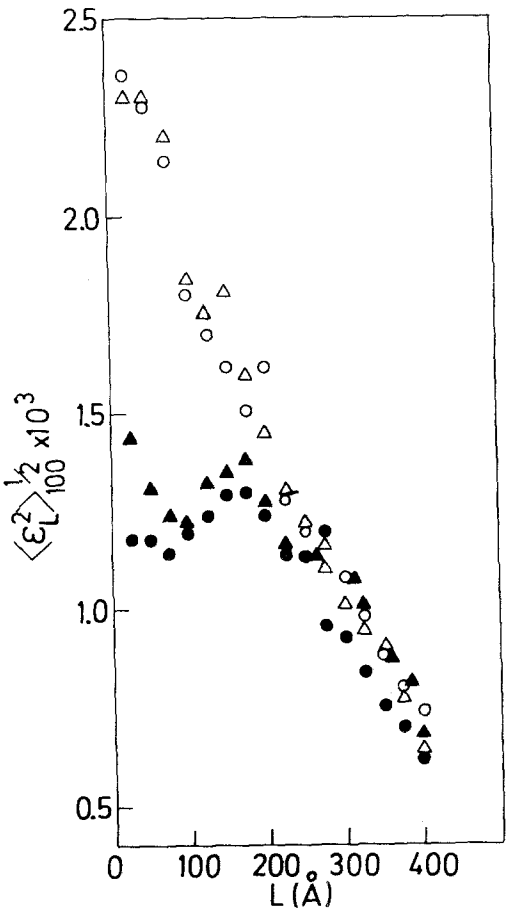

Figure 5 The root-mean square strains in direction [1 0 0] (marked (1) for higher intensity level and (2) for lower intensity level) obtained with two background levels of line (4 0 0) by means of two different standards (1S and 2S) versus L (distance normal to the diffracting planes): ▲ $\langle \epsilon_L^2 \rangle_{100}^{1/2}$(1) 1S, △ $\langle \epsilon_L^2 \rangle_{100}^{1/2}$(2) 2S, ● $\langle \epsilon_L^2 \rangle_{100}^{1/2}$(1) 1S, ○ $\langle \epsilon_L^2 \rangle_{100}^{1/2}$(2) 2S.

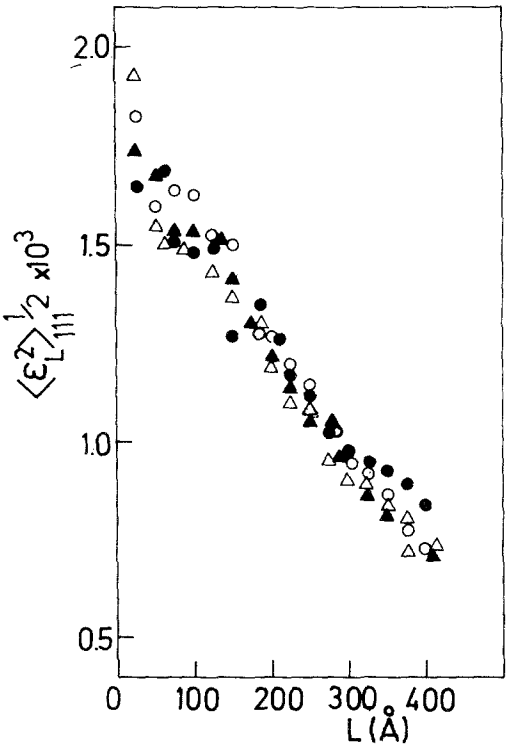

Figure 6 The root-mean square strains $\langle \epsilon_L^2 \rangle^{1/2}$ in direction [1 1 1] versus L. Two independent measurements analysed by means of two different standards are shown: △ $\langle \epsilon_L^2 \rangle_{111}^{1/2}$ 1S, ▲ $\langle \epsilon_L^2 \rangle_{111}^{1/2}$ 1S, ● $\langle \epsilon_L^2 \rangle_{111}^{1/2}$ 2S, ○ $\langle \epsilon_L^2 \rangle_{111}^{1/2}$ 2S.

produces the "hook" effect, and the obtained D_e values exceed the true values. The values of the effective domain sizes obtained when profiles are analysed using the second standard are lower by about 10 per cent than those obtained with the first standard.

In Fig. 5 the effect of an incorrectly chosen background of the second reflection is emphasized. It appears that the higher background level decreased the $\langle \epsilon_L^2 \rangle_{100}^{1/2}$ curves for low values of L, i.e. for values from 25 to 200 Å, while for the higher L values the effect of the incorrect background level is compensated for and the $\langle \epsilon_L^2 \rangle_{100}^{1/2}$ values fall on the same common curve. In Table II it can be seen that for the higher background level of line (4 0 0) the values $\langle \epsilon_L^2 \rangle_{100}^{1/2}$(1) at $L = 50$ Å are about half the values for the correctly chosen background level, for all annealing temperatures, reaching zero at 150° C and 300° C.

In Fig. 6 the root-mean square strains against L in direction [1 1 1] are shown for the Ag–8.2 at % Sn as-quenched samples. Two independent measurements are analysed using the two different standards, 1S and 2S. In the interval of L from 25 to 400 Å all the r.m.s. strain values fit the same curve well.

The errors due to the overestimation of the background level are more emphasized than are those resulting from the use of different annealed standards.

3.2. Peak asymmetry

Both twin (β) faults and extrinsic (α'') faults produce the asymmetric shape of the powder-pattern profiles, so that the centre of gravity of the peak is effected. Before actually evaluating the centre of gravity (CG), each peak height was divided by f^2 $(1 + \cos^2 2\theta / \sin^2 \theta)$ [16]. The $K\alpha_1$ line was resolved by applying the Rachinger correction [17]. The

TABLE III Comparison of measured stacking fault probabilities ($1.5\alpha + \beta$), obtained from line broadening analysis according to Equation 2 and of ($\beta + 4.5\alpha''$) obtained from the peak shift asymmetry Equation 3, with data of other authors.

Composition	Method	$(1.5\alpha + \beta)$	$(\beta + 4.5\alpha'')$
Ag 6 Sn	filings [6]	0.043	0.018
	splat-quenched	0.002	0.0038
Ag 8.2 Sn	splat-quenched	0.007	0.0055
Ag 9 Sn	filings [6]	0.094	0.037
	BC [5]		0.004–0.04
Ag 11 Sn	splat-quenched	0.005	0.0113

ratio of $K\alpha_1/K\alpha_2$ component was between 2 and 3, depending on the sample under examination.

Using (1 1 1) and (2 0 0) reflections, measured with Cu$K\alpha$ radiation, the displacement of the centre of gravity (ΔCG) according to [18] is given by

$$\Delta CG_{111} - \Delta CG_{200} = (11 \tan \theta_{111} + 14.6 \tan \theta_{200})(\beta + 4.5\alpha''). \quad (3)$$

The values of combined stacking fault probability ($\beta + 4.5\alpha''$) calculated from our measured data using Equation 3 are presented in Table I. The stacking fault probability ($\beta + 4.5\alpha''$) increased with increasing concentration of tin. This fact agrees with the results obtained from filings [6, 7] of the same alloy and with results obtained from solid solutions based on Cu, Ag, Ni, Al and Pb by other investigators [19]. The compound stacking fault probabilities $[1.5(\alpha' + \alpha'') + \beta]$, obtained from line broadening analysis according to Equation 2, agree only to within an order of magnitude with values obtained from peak asymmetry ($\beta + 4.5\alpha''$). This could be explained by the fact that all stacking faults of probabilities α', α'' and β are present, and also that small values of stacking fault probabilities, analysed according to Equation 3 and according to the separation of domain sizes calculated from Equation 2, would be fairly imprecise [20]. Our results with regard to the combined stacking fault probabilities of splat-quenched samples (Tables I and III) are included in the interval of values measured on bulk compressed samples of an Ag 9 Sn alloy [5] (Table III).

3.3. Peak position measurements

The lattice parameters a_{hkl}, calculated from the peak maximum positions 2θ of individual $(h\,k\,l)$ reflections, depend on the true lattice parameter a_0, the fault parameters $\alpha = \alpha' - \alpha''$, the residual stress σ, and the geometrical aberrations of the diffractometer. It has been shown [21] that these quantities are related according to

$$a_{hkl} = a_0 + G_{hkl} a_0 \alpha + S_1^{hkl} a_0 \sigma + m \cos\theta \cot\theta, \quad (4)$$

where G_{hkl} are constants which depend on the reflecting planes $(h\,k\,l)$ [13]. The elastic constants S_1^{hkl} are taken to be the average of the Reuss and Voigt values [22]. In our calculations, published elastic constants for Ag and Ag–3.17 at % Sn alloy were used [23] and were extrapolated to 6, 8.2 and 11 at % Sn, obtaining the following values of constants: -0.466×10^{-4}, -0.475×10^{-4} and -0.487×10^{-4} mm^2 N^{-1} (for Ag 6 Sn, Ag 8.2 Sn and Ag 11 Sn respectively).

The a_{hkl} values were measured at room temperature using a Seeman–Bohlin camera and Siemens diffractometer. In order to measure precisely the $2\theta_{hkl}$ position on a film a well annealed pure aluminium sample was used as standard. The examined sample was set in one half of the direct beam and the standard sample in the other.

The least square fit (LSQ) to Equation 4 was

TABLE IV Measured residual stresses σ_{LSQ} from Equation 4 and σ_A from Equation 5. (The samples analysed by means of a diffractometer were quenched by the two-piston method; the samples analysed using a Seeman–Bohlin camera were quenched by the piston and anvil technique).

	Composition	$d(\mu m)$	a_{app}(Å)	a_0(Å)	σ_A(N mm^{-2})	σ_{LSQ}(N mm^{-2})
Siemans diffractometer	Ag 6 Sn	30	4.111(0)	4.105(0)	−31.3	−14.2
	Ag 8.2 Sn	20	4.121(0)	4.117(1)	−14.8	−60.6
	Ag 11 Sn	30	4.132(0)	4.130(0)	− 9.9	− 2.6
Seeman–Bohlin camera	Ag 6 Sn	80	4.112(6)	4.104(7)	−40.2	−33.6
		45	4.137(0)	4.130(0)	−37.3	−29.8
	Ag 11 Sn	50	4.130(0)	4.135(0)	−24.9	−34.5
		90	4.132(5)	4.130(0)	−12.4	− 3.4

TABLE V Comparison of measured particle sizes D_{ehkl} and r.m.s. strains $\langle\epsilon_L^2\rangle_{hkl}^{1/2}(L = 50\ \text{Å})$ in directions [1 1 1] and [1 0 0] with data of other authors.

		Filings [6]		Filings [7]		BC [5]		Splat-quenched	
		$\langle\epsilon_L^2\rangle_{hkl}^{1/2} \times 10^3$	D_{ehkl}(Å)	$\langle\epsilon_L^2\rangle_{hkl}^{1/2} \times 10^3$	D_{ehkl}(Å)	$\langle\epsilon_L^2\rangle_{hkl}^{1/2} \times 10^3$	D_{ehkl}(Å)	$\langle\epsilon_L^2\rangle_{hkl}^{1/2} \times 10^3$	D_{ehkl}(Å)
Ag 6 Sn	[1 1 1]	3.8	135	3.1	170			0.85	1200
	[1 0 0]	5.5	75					1.06	900
Ag 8.2 Sn	[1 1 1]							1.7	520
	[1 0 0]							2.2	380
Ag 9 Sn	[1 1 1]	4.6	71	3.6	100	1.2	600		
	[1 0 0]	5.3	37				240		
Ag 11 Sn	[1 1 1]							1.44	770
	[1 0 0]							2.34	510

performed with all the terms included. The values obtained from the LSQ fit are presented in Table IV.

According to Wagner [13] it is possible to determine the apparent lattice parameter a_{app}, which also allows the calculation of the residual stress, σ_A, independently of α.

If a straight line is drawn through the points a_{hkl} so that it goes through the values of $(a_{420} + a_{311})/2$ and $(2a_{111} + a_{200})/3$, and it is extrapolated to $\cos\theta \cot\theta = 0$, a_{app} is obtained. For the annealed sample all the a_{hkl} values fall on the same straight line. In this case, by measuring a_{app} and a_0, the residual stress, σ_A, is obtained:

$$a_{app} - a_0 = [2(S_1)_{111} - S_1)_{200}] \frac{a_0 \sigma_A}{3}. \quad (5)$$

Assuming that the strains are produced by a constant elastic stress σ, Hooke's law can be applied so that: $\langle \epsilon_L^2 \rangle_{hkl}^{1/2} = \langle \sigma^2 \rangle^{1/2} / E_{hkl}$. Using measured r.m.s. strain for a large L, $\langle \epsilon_L^2 \rangle_{111}^{1/2} = 6 \times 10^{-4}$, and Young's modulus $E_{111} = 1.1 \times 10^{11}$ J m^{-2}, it is found that $\sigma = 71.6$ N mm^{-2}, i.e. the same order of magnitude as the residual stress measured from peak shifts (see Table IV). All measured values of a_{app} and a_0 are plotted in Fig. 7.

4. Results and discussion

4.1. Particle sizes and strains

In the splat-quenched Ag–Sn samples examined in the present work X-ray line broadening resulted from microstrains, reduction of the size of coherently diffracting domains, and stacking faults. Root-mean square strains and domain sizes are anisotropic. The anisotropy of effective particle sizes is partly a consequence of faulting, but the true size also influences its magnitude (the ratio of D_{e111}/D_{e100} is about 1.5). Using an electron microscope, stacking faults and crystallites of sizes between 700 and 1000 Å were also detected in Ag–6 Sn [24]. Extrinsic, intrinsic, twin faults and areas with a very high dislocation density, seen by the electron microscope, confirmed the findings in this work.

A comparison of the values of r.m.s. strains and domain sizes obtained by other authors from filings [6, 7] and bulk compressed (BC) samples [5], with those obtained in this paper, are given in Table V, while the values of stacking fault probabilities are given in Table III. The values of the r.m.s. strains and domain sizes of BC samples are comparable with those in splat-quenched samples (SQ).

For a number of metals root-mean square strains in directions [1 0 0] and [1 1 1] have been calculated [25] assuming a pure-screw or pure-edge character of dislocations in Au, Al, Cu, Ni, and the values reported as being between 1.03 and 1.34. In our measurements (Table I) these ratios were found to be 1.3, 1.3 and 1.6, respectively, and are within this theoretical interval of ratios.

4.1.1. Particle sizes and strains separated according to the single-profile method

From Table VI it can be seen that the values of the effective domain sizes D_{e111} and D_{e222} of Ag 8.2 Sn separated according to [14] compare with each other very well, as do also D_{e200} and D_{e400}. The least-square fit is much better for the first-order reflection than for the second. Also, the effective domain sizes in the directions [1 1 1] and [1 0 0] given for the as-quenched sample, using the Warren–Averbach separation, compare fairly well with the domain sizes of the single-profile method. The r.m.s. strains obtained by both methods are of the same order of magnitude, while the r.m.s. strains in directions [1 0 0] fit very well with the single profile values. From the results presented in Table VI it can be seen that both the Warren–Averbach and the single profile methods give comparable results for effective domain sizes and microstrains.

TABLE VI Separated effective domain sizes D_{ehkl} and root-mean square strains $\langle \epsilon^2 \rangle_{hkl}^{1/2}$ for $n = 1$, i.e. $L = 35$ Å according to the single-profile method, compared with the values obtained by the Warren–Averbach method.

hkl	N, n_0	a_0	a_1	a_2	D_e(Å)	$\frac{1}{N}\sum_{n_0}^{N}(A_n - P_n)^2$	$\langle \epsilon^2 \rangle_{hkl}^{1/2} \times 10^3$	Warren–Averbach	
								$\langle \epsilon^2 \rangle^{1/2} \times 10^3$	D_e(Å)
1 1 1	4, 2	1.127	−0.1308	0.0042	491	2.39×10^{-6}	3.80	1.73	520
2 0 0	4, 2	1.187	−0.1807	0.0056	273	2.42×10^{-4}	2.39	2.34	380
2 2 2	5, 1	1.152	−0.2210	0.0110	456	1.124×10^{-4}	2.94		
4 0 0	4, 2	1.200	−0.2570	0.0156	255	1.112×10^{-2}	2.91		

4.1.2. Isochronal annealing

The annealing study showed that the decrease of the r.m.s. strains $\langle \epsilon^2 \rangle^{1/2}$ in directions [1 1 1] and [1 0 0] (Figs. 1b and 2b) is fairly rapid as the annealing temperature rises. In Fig. 1a, it can be seen that D_{e111} values are larger for smaller concentrations of solute (Ag 6 Sn). It also appears that the effective domain sizes in Ag 6 Sn begin to grow at approximately 100° C, while in Ag 8.2 Sn and Ag 11 Sn this takes place at temperatures exceeding 200° C.

From the change in D_e, $\langle \epsilon^2 \rangle^{1/2}$ and $(1.5\alpha + \beta)$ taking place during annealing (Figs. 1a, b and 2a, b) conclusions can be drawn regarding the processes leading to recovery. Comparing the present results of isochronal annealing of D_{ehkl} and $\langle \epsilon^2 \rangle^{1/2}$ with those obtained from filings [7], it can be seen that they anneal in similar ways: after the first, constant stage, the domain sizes grow fairly rapidly with increasing annealing temperature while the r.m.s. strains decrease fairly abruptly, as the annealing temperature rises. The temperature at which the growth of domain sizes begins, increases with increasing solute concentration (see D_{e111} in Fig. 1a).

In general, the recovery both of r.m.s. strains and of the stacking fault probability α depends on the stacking fault energy of the respective material and on the deformation temperatures [26]. The recovery of the compound stacking fault probability $(1.5\alpha + \beta)$ is given in Fig. 2b.

Although the cause of deformation of filings [7] differs from that of the deformation of splat-cooled samples, it is evident that D_e and $\langle \epsilon^2 \rangle^{1/2}$ anneal in a similar way. It was though that in our samples the causes of deformation were thermal stresses and stresses caused by the shock of two pistons in collision.

The first recovery stage seen in the present work (Fig. 1) has also been observed in Ag–Sn [7], Cu–Ge [27, 18] and Cu–Al [29]. As has been suggested [7, 27], the first stage resembles a recovery process having a small (variable) activation energy, while the second is characteristic of recrystallization with an activation energy of a value near that for diffusion. Newton and Ruff [7] found the activation energy of the second stage to be 6 J mol^{-1}, which is slightly less than that for self-diffusion in Ag–Sn ($E_{\text{self-diff.}}$ in Ag–Sn = 8.8 J mol^{-1}). This activation energy is believed to be associated with recrystallization.

Since r.m.s. strains are connected with the elastic fields of dislocations, it is possible to interpret this recovery in terms of diminishing dislocation densities. In elastically anisotropic materials (the anisotropy factor of Ag–Sn varies from 3.27 to 3.35) both particle sizes and r.m.s. strains are responsible for changes in dislocation densities [30, 31].

4.2. Residual stress and lattice parameter changes

In Fig. 7 the lattice parameters of splat-quenched Ag–Sn alloys, filings [6] and bulk compressed Ag–Sn [5] alloys are plotted. From Fig. 7 it can be seen that in filings the a_{hkl} values of cold-worked and annealed samples are so distributed that they give a smaller value of the apparent lattice parameter a_{app} than the value of the true lattice parameter of the annealed sample a_0. For the bulk samples deformed by compression (BC), the variation in the difference between the apparent lattice parameter and the true lattice parameter was $a_{app} - a_0 > 0$. In general, the more plastic deformation, the greater was this difference. A similar behaviour has been observed in the difference in lattice parameters in Cu–1.35 at %

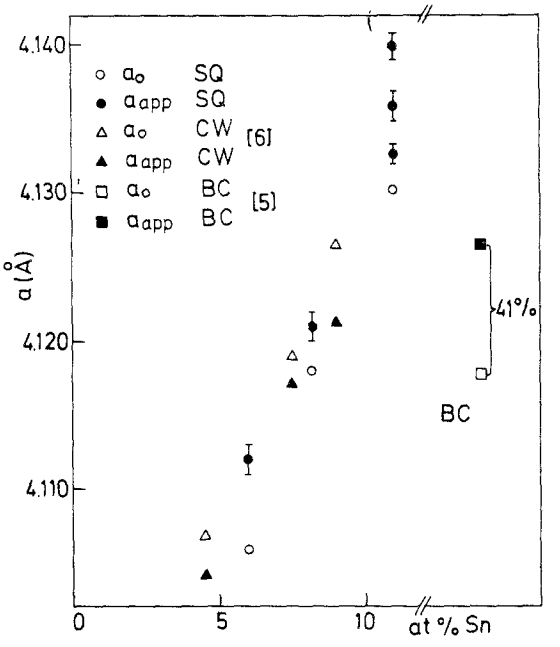

Figure 7 Variation of apparent lattice parameter a_{app} and lattice parameter a_0 of annealed Ag–Sn alloys with concentration of tin: ○ a_0 splat-quenched (SQ), • a_{app} splat-quenched, △ a_0 filings (CW), ▲ a_{app} filings, □ a_0 bulk compressed (BC), ■ a_{app} bulk compressed (on the right are shown a_0 and a_{app} for one stage of deformation of bulk compressed samples. The reduction in thickness is indicated in per cent).

Sn deformed in compression [32]. The behaviour of lattice parameters in Cu–2.6 at % Sn, deformed in tension, shows $a_0 - a_{app} > 0$ [33]. This difference increases with increasing plastic deformation. Davies and Wagner [34] have studied tensile deformation in a bulk polycrystalline Ag–30 at % Cd alloy. For each state of tensile strain, they determined the applied stress σ_A from the lattice parameter a_{app} which is smaller than a_0 of the annealed sample. All this work lends support to the conclusion that the difference in lattice parameter $a_{app} - a_0 > 0$ obtained in SQ samples in the present investigation is due to compressive residual surface stresses.

As has been shown [5, 32, 33, 34], for certain alloy concentrations the absolute value of the surface residual stress is higher for greater plastic deformation due to tension or compression. From Fig. 7 and Table IV it can be seen that the thinner splat-quenched samples have a higher apparent lattice parameter and thus also higher surface residual stresses. Grant has shown [35] that, in splat-quenching, thinner samples are quenched with a higher cooling rate than thicker samples. Thus, our results show that the more successful the quenching is, the more the sample will be plastically deformed. From the residual stress values presented in Table IV it can be seen that for different thicknesses (45, 50 and 90 μm) of the same alloy (Ag 11 Sn) different values are obtained ($\sigma_{LSQ} = -35.5, -29.8$ and $-3.4\,N\,mm^{-2}$ respectively). Comparing σ_{LSQ} values from Table IV with each other, it is found that for the Ag 8.2 Sn sample analysed by means of a diffractometer, the σ_{LSQ} value is higher than it is for the samples of other concentrations. This fact suggests that this sample was better quenched than the others. However, the findings obtained from filings [6] which show that r.m.s. strain increases and D_e decreases in directions [1 1 1] and [1 0 0] as the solute content increases, do not agree completely with our results. It is thought that this disagreement is caused by quenching, and so the r.m.s. strain values of Ag 8.2 Sn are higher and the effective domain sizes and true domain sizes lower, than those of Ag 11 Sn.

5. Conclusions

In this work the broadening and the shifts of X-ray diffraction peaks of splat-quenched Ag–Sn alloys were studied. From the Stokes-corrected Fourier coefficients of pure diffraction profiles, the particle sizes and microstrain components were separated using the Warren–Averbach and the single profile methods. The following conclusions were drawn:

The peak broadening was due to microscopic strains, particle sizes and stacking faults. The microstrains and particle sizes were anisotropic and this anisotropy may be attributed to stacking faults and the non-uniform distribution of dislocation.

The intrinsic, extrinsic and twin faults were found and were confirmed by electron microscope observation. A very high and irregular dislocation density was also detected.

The peak shift analysis gives evidence of the existence of residual compressive macrostresses which remained in the samples after the plastic deformation caused by quenching. Better quenching gave thinner samples and higher macrostresses.

Acknowledgement

The authors are grateful to Dr A. Kirin for help and discussions during the work.

References

1. G. THOMAS and R. H. WILLENS, *Acta Met.* **12** (1964) 191.
2. A. M. TONEJC and D. KUNSTELJ, *Fizika* 8 (1976) 194.
3. J. DIXMIER and A. GUINIER, *Mém. Scient. Rev. Metall.* **64** (1967) 53.
4. A. M. TONEJC, A. KIRIN and A. BONEFAČIĆ, *Fizika* 8 (1976) 87.
5. R. P. J. ADLER and C. N. J. WAGNER, *Met. Trans.* **1** (1970) 2791.
6. *Idem, J. Appl. Phys.* **33** (1962) 3451.
7. C. J. NEWTON and A. W. RUFF Jr, *Met. Trans.* **1** (1970) 2833.
8. A. R. STOKES, *Proc. Phys. Soc. London* **61** (1948) 382.
9. B. E. WARREN and B. L. AVERBACH, *J. Appl. Phys.* **21** (1950) 595; *idem, ibid.* **23** (1952) 497.
10. A. GANGULEE, *J. Appl. Cryst.* 7 (1974) 434.
11. B. E. WARREN, *Progress Met. Phys.* 8 (1959) 147.
12. N. C. HALDER and C. N. J. WAGNER, *Adv. X-ray Analysis* 9 (1966) 91.
13. C. N. J. WAGNER, "Local Atomic Arrangements Studied by X-ray Diffraction" (Gordon and Breach, New York, 1966) pp. 219 and 255.
14. J. MIGNOT and D. RONDOT, *Acta Met.* **23** (1975) 1321.
15. G. GILLI and P. A. BOREA, *J. Appl. Cryst.* **3** (1970) 205.
16. H. P. KLUG and L. E. ALEXANDER, "X-ray Diffraction Procedures" (John Wiley and Sons, New York, 1974) p. 167.
17. W. A. RACHINGER, *J. Sci. Instrum.* **25** (1948) 254; *idem, ibid.* **25** (1948) 353.
18. J. B. COHEN and C. N. J. WAGNER, *J. Appl. Phys.*

33 (1962) 2073.
19. L. DELEHOUZÉE and A. DERUYTTERE, *Acta Met.* **15** (1967) 727.
20. S. P. SEN GUPTA and M. DE, *J. Appl. Cryst.* **3** (1970) 410.
21. C. N. J. WAGNER, J. P. BOISSEAU and E. A. AQUA, *Trans. Met. Soc. AIME* **233** (1965) 1280.
22. G. B. GREENOUGH, *Prog. Met. Phys.* **3** (1952) 176.
23. G. SIMONS and H. WANG, "Single Crystal Elastic Constants and Calculated Aggregate Properties: A. Handbook" (The M.I.T. Press, London, 1971) pp. 86 and 90.
24. D. KUNSTELJ and A. BONEFAČIĆ, *Proc. Yug. Centre of Crystall.* **10** (1975) 80.
25. FU-WEN LING and E. A. STARKE, *J. Appl. Cryst.* **3** (1970) 407.
26. P. C. J. GALLAGHER, *Met. Trans.* **1** (1970) 2429.
27. J. W. KIRBY, D. J. BORICH and D. E. MIKKOLA, *ibid.* **4** (1973) 1129.
28. W. G. TRUCKNER and D. E. MIKKOLA, *J. Appl. Phys.* **40** (1969) 5021.
29. D. E. MIKKOLA and J. B. COHEN, *ibid.* **33** (1962) 892.
30. G. K. WILLIAMSON and R. E. SMALLMAN, *Phil. Mag.* **1** (1956) 34.
31. R. E. SMALLMAN and K. H. WESTMACOTT, *ibid.* **2** (1957) 669.
32. J. MIGNOT and D. RONDOT, *J. Appl. Cryst.* **6** (1973) 447.
33. A. PAUVERT, Thèsis, Besançon (1974).
34. H. A. DAVIES and C. N. J. WAGNER, *J. Mater. Sci.* **7** (1972) 105.
35. J. N. GRANT, *Fizika* **2**, *Suppl. 2* (1970) 16.1.

Received 3 May and accepted 19 July 1979.